



Thermal transients in a capillary evaporator prior to the initiation of boiling

Tim J. LaClair, Issam Mudawar*

Boiling and Two-Phase Flow Laboratory, School of Mechanical Engineering, Purdue University, West Lafayette, IN 47907, USA

Received 27 May 1999; received in revised form 26 January 2000

Abstract

A solution for the temperature profile in a cylindrical capillary evaporator subject to a uniform heat flux prior to the initiation of boiling is derived using the Green's Function method. An approximate solution is also derived for the case in which the evaporator is heated by means of a constant conductance to a heat dissipating device. The results of the analysis allow for the determination of applied power levels for which nucleation is likely to occur only within the vapor grooves of the evaporator while maintaining subcooling in the liquid core, thereby increasing the likelihood of a successful startup. Also, limits are found for which additional increases in the applied heat flux do not increase the temperature difference between the vapor grooves and the wick–liquid core interface. Several advantages of larger diameter evaporators observed experimentally in startup are explained and quantified by the model. This analysis is appropriate for standard capillary pumped loop evaporators during a fully-flooded startup as well as starter pump designs and loop heat pipes. © 2000 Elsevier Science Ltd. All rights reserved.

1. Introduction

The Capillary Pumped Loop (CPL) is a two-phase thermal control device that is capable of passively transporting heat over large distances with minimal temperature losses. Although earth-based applications of the CPL have been proposed, it is especially well suited for thermal management in spacecraft, where gravity and hence its potentially deleterious effects on the CPL's operation are absent. The CPL uses capillary action for fluid transport and contains no moving parts. A derivative of the heat pipe, it possesses several features that make it an attractive design alternative in several circumstances. Multiple evaporators and con-

densers can be added at different locations in a CPL, allowing the use of a single loop to reject heat from multiple sources to multiple sinks, possibly at different temperatures. In contrast to the heat pipe, wicks are absent in most of the transport section of the CPL. Instead, liquid and vapor flow through smooth walled tubing, thereby reducing the frictional pressure losses and increasing the maximum potential fluid flow and heat transfer rates.

A CPL in its most basic form is presented in Fig. 1. During normal operation heat is applied to the evaporator, which causes the working fluid to evaporate. The wick supplies liquid to the evaporator walls while vapor is generated at the interface between the wick structure and the vapor grooves, as shown in Fig. 2. A meniscus forms at the liquid–vapor interface, which results in a pressure differential between the two phases equal to the capillary pressure $2\sigma/r$. This pressure difference pro-

* Corresponding author. Tel.: +1-765-494-5705; fax: +1-765-494-0539.

E-mail address: mudawar@ecn.purdue.edu (I. Mudawar).

Nomenclature

a	liquid core radius	T_i	temperature in region i
A_e	evaporator surface area	T_m	temperature of a thermal mass
A_{in}	constant in each eigenfunction ψ_{in}	T_{sat}	saturation temperature
b	radius at interface between wick and vapor grooves	T^*	normalized temperature profile
B_{in}	constant in each eigenfunction ψ_{in}	\tilde{T}_b	temperature function defined in Eq. (28)
c	outer radius of evaporator	ΔT_{gc}^*	normalized temperature difference defined in Eq. (32)
c_p	specific heat	$\Delta T_{gc, incip}$	temperature difference between vapor grooves and liquid core at incipience
C_e	thermal capacitance of evaporator	$\Delta T_{sub, 0}$	initial subcooling in evaporator
C_m	thermal capacitance of thermal mass	U	overall heat transfer coefficient
f_i	initial temperature in region i for homogeneous problem	Y_0, Y_1	Bessel functions of order zero and one of the 2nd kind
G_{ij}	Green's function in region i due to a source in region j		
i	index taking the values 1, 2, 3		
J_0, J_1	Bessel functions of order zero and one of the 1st kind	<i>Greek symbols</i>	
K_1, K_2	constants defined in Eq. (8b)	α_i	thermal diffusivity of material i
k_i	thermal conductivity of material i	α_w	bulk thermal diffusivity of wick material
k_w	bulk thermal conductivity of wick material	β_n	n th eigenvalue
n	index	Δ	thermal capacitance per unit length
N_n	constant defined in Eqs. (11b) and (11c)	γ_j	constant defined in Eq. (8b)
q''	heat flux	η_n	non-dimensional eigenvalue defined in Eq. (8b)
\dot{Q}	heat dissipation rate in thermal mass	φ	porosity
r	radius	ρ	density
r'	a radius variable in the Green's function	σ	surface tension
R_c	thermal capacitance ratio	τ	a time variable in the Green's function
R_i	region i	ψ_{in}	n th eigenfunction in region i
t	time	ξ	parameter defined in Eq. (24c)
t_1	time when nucleation is expected	<i>Subscripts</i>	
T	temperature	f	fluid
T_0	initial temperature	m	mixture
		s	solid

vides the force that drives the fluid flow through the entire loop. The vapor flows through the vapor grooves, out of the evaporator, through the vapor transport lines, and into the condenser, where it condenses into liquid. Liquid condensate continues to flow through the liquid transport lines and returns to the evaporator, completing the cycle. The two-phase reservoir is used to control the temperature of the loop and accommodates fluid inventory shifts during changes in operating conditions. It is typically thermostatically controlled to maintain a constant temperature setpoint, and in steady-state operation, a state of thermodynamic equilibrium results in which the pressure of the reservoir equals the saturation pressure corresponding to the temperature setpoint. The pressure of the reservoir effectively biases the pressure of the entire loop

since pressure losses in the reservoir line are negligible. In this manner, the pressure of the loop, and thus its saturation temperature, is nearly the same as that of the reservoir.

The CPL is becoming a favorite design for spacecraft thermal control due to its ability to transport large heat loads and the promise of operating as a centralized thermal bus using multiple parallel evaporators. CPL development began in the 1960s and has been quite active since the 1980s. Excellent reviews of the development history and theory of operation are available in the literature [1,2]. In recent years, numerous CPLs have been fabricated and ground-tested, several have been tested in flight experiments and designs have been selected for use on a few spacecraft missions [3]. Nevertheless, issues relating to the CPL's reliability and robustness have limited its acceptance and im-

plementation, and have been the primary focus of research in recent years [4–7].

One problem which has plagued CPLs in both ground and flight tests is the difficulty in starting the evaporators. Typically, after a CPL successfully starts and enters into a steady operation mode it performs quite well and the operation is fairly predictable. However, before steady state operation can occur, a series of transient events, collectively referred to as the *startup*, must take place where the thermophysical state of fluid through much of the loop changes quite dramatically. During the startup, the locations occupied by liquid and vapor transiently shift to those corresponding to steady state operation. This repositioning of liquid and vapor occurs through the combined processes of vaporization, condensation, and multi-phase fluid flow through various portions of the loop.

In theory, vapor should form only in the vapor grooves of an evaporator. However, if sufficient superheat develops in the grooves before nucleation occurs, the wick and possibly the liquid core can also heat up to a temperature that is greater than the saturation temperature, and nucleation could potentially occur there as well. Additionally, vapor may be forced through the wick and injected into the liquid core during the initial pressure spike or pressure surge of the startup. If the temperature of the liquid core is at a temperature near or at saturation, then vapor may remain there without condensing and in some cases may actually grow. Vapor presence in the liquid core has been found to fully or partially block liquid flow to the wick, which may lead eventually to deprime — the loss of capillary pumping action — of an evaporator [8,9]. Also, vapor presence in the evaporator core has been found to influence pressure oscillations in the

CPL [10]. Further aspects of CPL startup, which are beyond the scope of this paper, are discussed in [8,9].

The preheating stage of the evaporator, before vapor forms, has received relatively little attention in the past. This is the first stage of startup in *an evaporator that is initially fully-flooded with liquid*, and occurs not only in the fully-flooded startup of a traditional evaporator, but also in starter pumps (evaporators plumbed with a third port that connects the liquid core directly to the reservoir) and loop heat pipe (LHP) evaporators. The temperature profile of an evaporator at the termination of the preheating stage, i.e. at the commencement of boiling, determines if nucleation and vapor phase longevity are possible at locations other than inside the vapor flow passages. To some degree this profile will also affect later thermal and fluid processes during the startup and continued operation, and it can be used as a starting point in the analysis of post-nucleation phenomena. A numerical simulation of the preheating stage was performed by Li and Ochterbeck [11] for an evaporator with a Cartesian geometry. The geometry of the vapor grooves was included in the analysis and temperature dependent thermal properties were used. Li and Ochterbeck compared the numerical results with those of an experimental study using flow visualization performed in the

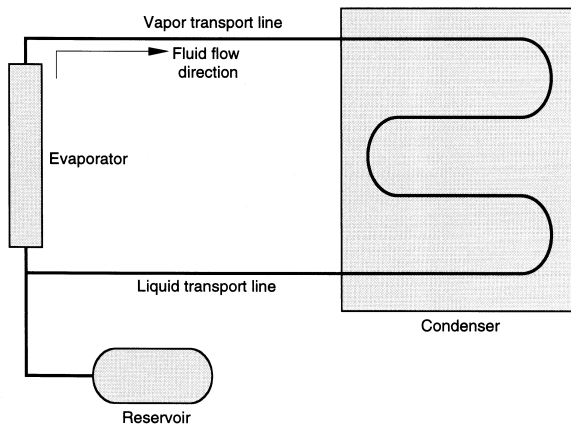


Fig. 1. Basic capillary pumped loop design.

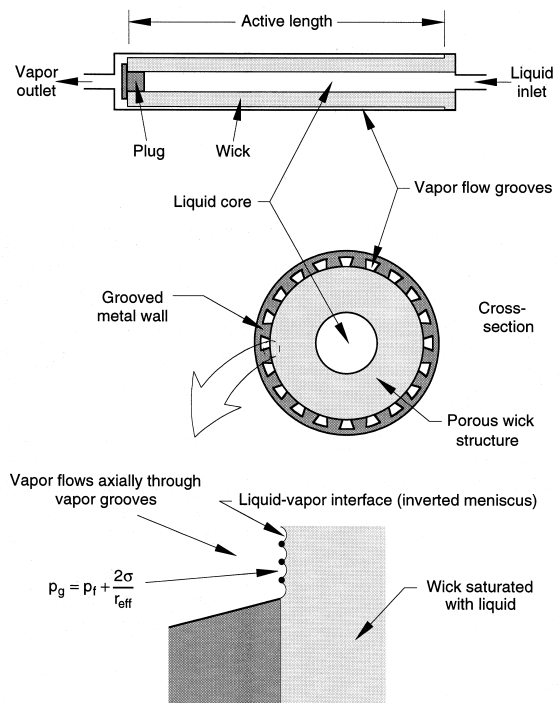


Fig. 2. Evaporator design and groove detail showing menisci at liquid–vapor interface at wick surface.

same investigation in which an evaporator with the same geometry was used.

In this paper, an analytical model of conduction during the initial heating of a cylindrical capillary evaporator is presented that is applicable to standard CPL evaporators, starter pumps, and also loop heat pipes. The boundary conditions of (1) constant applied heat flux and (2) conduction to a thermal mass with a non-negligible thermal capacitance that dissipates heat are both considered and the results for the two cases compared. Focus is placed upon the temperature difference between the vapor grooves and the liquid core, and heating conditions that optimize this temperature difference are deduced. The primary objectives of this study are to determine the temperature profile when boiling commences and evaluate the influence of the applied heat flux level on this profile. This paper also addresses differences in the observed startup behavior between large and small evaporators, and the startup performance of evaporators that use a metal wick is evaluated.

2. Analysis

To obtain the temperature profile during the initial heating of a cylindrical capillary evaporator, several assumptions are made that allow a solution to be obtained analytically. These assumptions are not highly restrictive, yet they lead to an analytical representation for the temperature profile of the evaporator which yields several insights into the CPL startup, and several results are derived which would not be evident from a purely numerical study. This approach provides a solution that can be applied to a number of different designs by simply altering the parameters in the model. This approach was pursued with the overall goal of obtaining generalized conclusions about the preheat phase of a capillary evaporator startup.

As a first assumption, the vapor groove geometry is neglected in the conduction model and a simple three layer composite cylindrical structure is assumed for the capillary evaporator. Because of the typically slow thermal transients during this preheating stage in an evaporator, the temperature of liquid in the vapor grooves will not vary significantly with position, but rather will be approximately uniform. Also, in most evaporators, the wick and liquid thermal properties do not vary substantially from one another, so that the liquid present in the vapor grooves may be considered an extension of the liquid-saturated wick (this assumption will be substantiated with property data in the next section). By selecting an appropriate inner radius for the metal wall of the evaporator in the model, the contact area between the metal wall and the vapor grooves and wick can be effectively approximated.

Fig. 3 shows the actual and assumed geometries. The second assumption is that the heat flux to the evaporator is applied uniformly to the circumference of the evaporator. Since the metal wall typically has a high thermal conductivity, any non-uniformity in the actual heat flux at the outer radius will be minimized at the wick to wall interface. Thirdly, constant thermal properties are assumed in the analysis, and average properties for the liquid-saturated wick are used. In view of the other uncertainties in the model, the use of variable properties would only confuse the results. Since the fluid is not being pumped during the first stage of heating, the dominant heat transfer mechanism is conduction; convection is negligible, particularly in a microgravity environment.

A two-dimensional analysis is used throughout this investigation. Because the active length of a capillary evaporator represents the greater part of the total length and the entire length is heated, the two-dimensional radial system is appropriate. For a cylinder that is heated with a uniform heat flux along the lateral surface and perfectly insulated at the ends, the three-dimensional problem reduces exactly to the two-dimensional case. The end effects resulting from the region beyond the active length of the evaporator is not

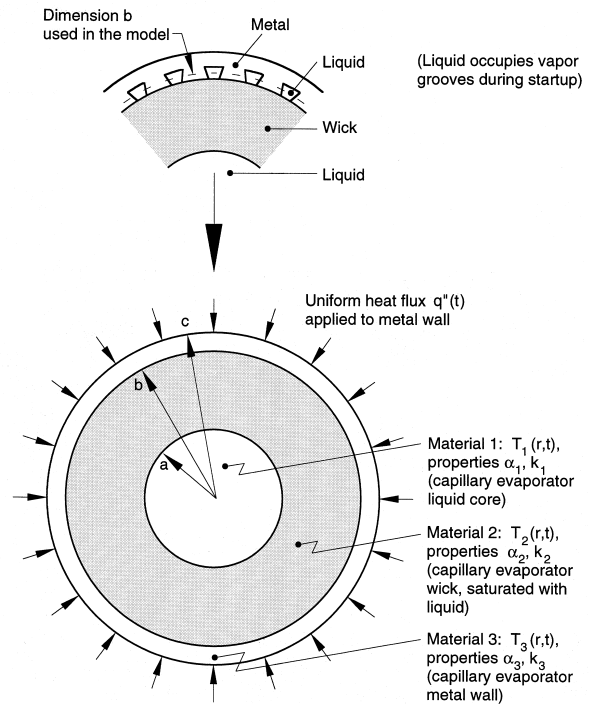


Fig. 3. Actual evaporator groove geometry and the three-layer composite cylinder geometry used in the thermal conduction model of the evaporator during a fully-flooded startup.

expected to significantly alter the results of this analysis.

Since no solution for the three-layer composite cylinder subject to a uniform applied heat flux appears in the literature, a new solution is derived. To begin the analysis, the mathematical formulation of the transient conduction problem under consideration is specified as follows. A cylinder is composed of three materials as shown in Fig. 3. Material 1 (liquid core), in the region R_1 given by $0 \leq r < a$, is at temperature $T_1(r, t)$; material 2 (wick saturated with liquid), in the region R_2 defined by $a < r < b$, is at temperature $T_2(r, t)$; and material 3 (metal wall), in the region R_3 defined by $b < r < c$, is at temperature $T_3(r, t)$. A uniform heat flux $q''(t)$ is applied at the outer radius c . The differential equation corresponding to this problem is given by the following:

$$\frac{1}{\alpha_i} \frac{\partial T_i}{\partial t} = \frac{1}{r} \frac{\partial}{\partial r} \left(r \frac{\partial T_i}{\partial r} \right) \quad (1)$$

in each region R_i , $i = 1, 2, 3$. Continuity of the heat flux and of temperature is required at each interface between regions. This results in the following interface boundary conditions:

$$k_1 \frac{\partial T_1}{\partial r} = k_2 \frac{\partial T_2}{\partial r} \quad \text{at } r = a, \quad (2a)$$

$$T_1(r, t) = T_2(r, t) \quad \text{at } r = a, \quad (2b)$$

$$k_2 \frac{\partial T_2}{\partial r} = k_3 \frac{\partial T_3}{\partial r} \quad \text{at } r = b, \quad (2c)$$

$$T_2(r, t) = T_3(r, t) \quad \text{at } r = b. \quad (2d)$$

Also, there exists a symmetry boundary condition at the center of the cylinder and a boundary condition corresponding to an applied heat flux at the outer radius:

$$\frac{\partial T_1}{\partial r} = 0 \quad \text{at } r = 0 \quad (2e)$$

$$k_3 \frac{\partial T_3}{\partial r} = q''(t) \quad \text{at } r = c. \quad (2f)$$

As an initial condition, a uniform temperature is assumed everywhere in the composite cylinder,

$$T_i(r, t) = T_0 \quad \text{for } t = 0, i = 1, 2, 3. \quad (2g)$$

The Green's function shall be derived for this problem by first considering the homogeneous problem with an arbitrary initial condition [12]. Specifically, the following problem is solved:

$$\frac{1}{\alpha_i} \frac{\partial T_i}{\partial t} = \frac{1}{r} \frac{\partial}{\partial r} \left(r \frac{\partial T_i}{\partial r} \right), \quad i = 1, 2, 3. \quad (3a)$$

The homogeneous boundary conditions are

$$\frac{\partial T_1}{\partial r} \Big|_{r=0} = \frac{\partial T_3}{\partial r} \Big|_{r=c} = 0. \quad (3b)$$

The interfacial conditions are identical to those given by Eqs. (2a)–(2d). The initial conditions are given by the following:

$$T_i(r, t = 0) = f_i(r), \quad i = 1, 2, 3. \quad (3c)$$

The solution is obtained by the separation of variables approach, which results in the following eigenvalue problem:

$$\frac{1}{r} \frac{d}{dr} \left(r \frac{d\psi_{in}}{dr} \right) + \frac{\beta_n^2}{\alpha_i} \psi_{in} = 0 \quad (4a)$$

in each region R_i , subject to the boundary conditions

$$\frac{d\psi_{1n}}{dr} = 0 \quad \text{at } r = 0 \quad (4b)$$

$$\psi_{1n}(r) = \psi_{2n}(r) \quad \text{at } r = a \quad (4c)$$

$$k_1 \frac{d\psi_{1n}}{dr} = k_2 \frac{d\psi_{2n}}{dr} \quad \text{at } r = a \quad (4d)$$

$$\psi_{2n}(r) = \psi_{3n}(r) \quad \text{at } r = b \quad (4e)$$

$$k_2 \frac{d\psi_{2n}}{dr} = k_3 \frac{d\psi_{3n}}{dr} \quad \text{at } r = b \quad (4f)$$

$$\frac{d\psi_{3n}}{dr} = 0 \quad \text{at } r = c. \quad (4g)$$

The eigenvalue $\beta_0 = 0$ is treated first. The corresponding eigenfunctions are given by

$$\psi_{j0}(r) = A_{j0} + B_{j0} \ln r. \quad (5a)$$

Eq. (4b), along with the physical requirement that the temperature remain bounded, requires that the coefficient

$$B_{10} = 0 \quad (5b)$$

so that

$$\psi_{10}(r) = A_{10} \quad (5c)$$

Application of the boundary conditions given by Eqs. (4d) and (4f) results in

$$B_{30} = B_{20} = 0, \quad (5d)$$

and Eqs. (4c) and (4e) now require that

$$A_{10} = A_{20} = A_{30} = A_0. \tag{5e}$$

Therefore, the eigenfunctions corresponding to the eigenvalue $\beta_0 = 0$ are constant and are equal in all regions:

$$\psi_{i0}(r) = A_0, \quad i = 1, 2, 3. \tag{5f}$$

For positive eigenvalues β_n , the general solution of Eq. (4a) is given by

$$\psi_{in}(r) = A_{in}J_0\left(\frac{\beta_n}{\sqrt{\alpha_i}}r\right) + B_{in}Y_0\left(\frac{\beta_n}{\sqrt{\alpha_i}}r\right), \tag{6}$$

$i = 1, 2, 3$

where $J_0(r)$ and $Y_0(r)$ are Bessel functions of order zero of the 1st and 2nd kind, respectively. The boundary condition given by Eq. (4a) requires that

$$\begin{aligned} A_{2n}J_0\left(\frac{\beta_n}{\sqrt{\alpha_2}}b\right) + B_{2n}Y_0\left(\frac{\beta_n}{\sqrt{\alpha_2}}b\right) \\ = A_{3n}J_0\left(\frac{\beta_n}{\sqrt{\alpha_3}}b\right) + B_{3n}Y_0\left(\frac{\beta_n}{\sqrt{\alpha_3}}b\right) \end{aligned} \tag{7d}$$

$$\begin{aligned} \frac{k_2}{k_3}\sqrt{\frac{\alpha_3}{\alpha_2}}\left\{A_{2n}J_1\left(\frac{\beta_n}{\sqrt{\alpha_2}}b\right) + B_{2n}Y_1\left(\frac{\beta_n}{\sqrt{\alpha_2}}b\right)\right\} \\ = A_{3n}J_1\left(\frac{\beta_n}{\sqrt{\alpha_3}}b\right) + B_{3n}Y_1\left(\frac{\beta_n}{\sqrt{\alpha_3}}b\right) \end{aligned} \tag{7e}$$

$$A_{3n}J_1\left(\frac{\beta_n}{\sqrt{\alpha_3}}c\right) + B_{3n}Y_1\left(\frac{\beta_n}{\sqrt{\alpha_3}}c\right) = 0 \tag{7f}$$

where $J_1(r)$ and $Y_1(r)$ are Bessel functions of order one of the 1st and 2nd kind, respectively. These five equations can be written in matrix form as

$$\begin{bmatrix} J_0\left(\gamma_1\frac{a}{c}\eta_n\right) & -J_0\left(\gamma_2\frac{a}{c}\eta_n\right) & -Y_0\left(\gamma_2\frac{a}{c}\eta_n\right) & 0 & 0 \\ K_1J_1\left(\gamma_1\frac{a}{c}\eta_n\right) & -J_1\left(\gamma_2\frac{a}{c}\eta_n\right) & -Y_1\left(\gamma_2\frac{a}{c}\eta_n\right) & 0 & 0 \\ 0 & J_0\left(\gamma_2\frac{b}{c}\eta_n\right) & Y_0\left(\gamma_2\frac{b}{c}\eta_n\right) & -J_0\left(\frac{b}{c}\eta_n\right) & -Y_0\left(\frac{b}{c}\eta_n\right) \\ 0 & K_2J_1\left(\gamma_2\frac{b}{c}\eta_n\right) & K_2Y_1\left(\gamma_2\frac{b}{c}\eta_n\right) & -J_1\left(\frac{b}{c}\eta_n\right) & -Y_1\left(\frac{b}{c}\eta_n\right) \\ 0 & 0 & 0 & J_1(\eta_n) & Y_1(\eta_n) \end{bmatrix} \begin{bmatrix} 1 \\ A_{2n} \\ B_{2n} \\ A_{3n} \\ B_{3n} \end{bmatrix} = \begin{bmatrix} 0 \\ 0 \\ 0 \\ 0 \\ 0 \end{bmatrix} \tag{8a}$$

$$B_{1n} = 0. \tag{7a}$$

The constant A_{1n} is set to unity, $A_{1n} = 1$, without loss of generality, as discussed in [12]. Application of the remaining boundary conditions, Eqs. (4c)–(4g), respectively, leads to the following equations:

$$J_0\left(\frac{\beta_n}{\sqrt{\alpha_1}}a\right) = A_{2n}J_0\left(\frac{\beta_n}{\sqrt{\alpha_2}}a\right) + B_{2n}Y_0\left(\frac{\beta_n}{\sqrt{\alpha_2}}a\right) \tag{7b}$$

$$\frac{k_1}{k_2}\sqrt{\frac{\alpha_2}{\alpha_1}}J_1\left(\frac{\beta_n}{\sqrt{\alpha_1}}a\right) = A_{2n}J_1\left(\frac{\beta_n}{\sqrt{\alpha_2}}a\right) + B_{2n}Y_1\left(\frac{\beta_n}{\sqrt{\alpha_2}}a\right) \tag{7c}$$

where

$$\eta_n = \frac{\beta_n}{\sqrt{\alpha_3}}c, \quad \gamma_j = \sqrt{\frac{\alpha_3}{\alpha_j}} \quad (j = 1, 2)$$

$$K_1 = \frac{k_1}{k_2}\sqrt{\frac{\alpha_2}{\alpha_1}} \quad \text{and} \quad K_2 = \frac{k_2}{k_3}\sqrt{\frac{\alpha_3}{\alpha_2}} \tag{8b}$$

Including the ratios a/c and b/c , there are six non-dimensional parameters, which depend on the properties and dimensions of the particular problem, appearing in Eq. (8a). The eigenvalues for the problem are obtained by setting the determinant of the matrix in Eq. (8a) equal to zero:

$$\det \begin{vmatrix} J_0\left(\gamma_1 \frac{a}{c} \eta_n\right) & -J_0\left(\gamma_2 \frac{a}{c} \eta_n\right) & -Y_0\left(\gamma_2 \frac{a}{c} \eta_n\right) & 0 & 0 \\ K_1 J_1\left(\gamma_1 \frac{a}{c} \eta_n\right) & -J_1\left(\gamma_2 \frac{a}{c} \eta_n\right) & -Y_1\left(\gamma_2 \frac{a}{c} \eta_n\right) & 0 & 0 \\ 0 & J_0\left(\gamma_2 \frac{b}{c} \eta_n\right) & Y_0\left(\gamma_2 \frac{b}{c} \eta_n\right) & -J_0\left(\frac{b}{c} \eta_n\right) & -Y_0\left(\frac{b}{c} \eta_n\right) \\ 0 & K_2 J_1\left(\gamma_2 \frac{b}{c} \eta_n\right) & K_2 Y_1\left(\gamma_2 \frac{b}{c} \eta_n\right) & -J_1\left(\frac{b}{c} \eta_n\right) & -Y_1\left(\frac{b}{c} \eta_n\right) \\ 0 & 0 & 0 & J_1(\eta_n) & Y_1(\eta_n) \end{vmatrix} = 0 \tag{9}$$

This determinant is simply a function of the variable η_n with various sums of products of Bessel functions. Although solution of the equation may appear to be a somewhat daunting task, the numerical values of the non-dimensional eigenvalues, which are the roots of this equation, can be calculated quite simply using a symbolic software package such as Mathematica[®], Mathcad[®], or Maple.

Once the eigenvalues are determined, the coefficients A_{in} and B_{in} can be determined by solving any four of the five equations given by Eqs. (7b)–(7f). Using the last four,

$$\sum_{n=1}^{\infty} \frac{1}{N_n} e^{-\beta_n^2 t} \psi_{in}(r) \left\{ \frac{k_1}{\alpha_1} \int_0^a r' \psi_{1n}(r') f_1(r') dr' + \frac{k_2}{\alpha_2} \int_a^b r' \psi_{2n}(r') f_2(r') dr' + \frac{k_3}{\alpha_3} \int_b^c r' \psi_{3n}(r') f_3(r') dr' \right\} \tag{11a}$$

for $i = 1, 2, 3$, where

$$\begin{bmatrix} A_{2n} \\ B_{2n} \\ A_{3n} \\ B_{3n} \end{bmatrix} = \begin{bmatrix} J_1\left(\gamma_2 \frac{a}{c} \eta_n\right) & Y_1\left(\gamma_2 \frac{a}{c} \eta_n\right) & 0 & 0 \\ J_0\left(\gamma_2 \frac{b}{c} \eta_n\right) & Y_0\left(\gamma_2 \frac{b}{c} \eta_n\right) & -J_0\left(\frac{b}{c} \eta_n\right) & -Y_0\left(\frac{b}{c} \eta_n\right) \\ K_2 J_1\left(\gamma_2 \frac{b}{c} \eta_n\right) & K_2 Y_1\left(\gamma_2 \frac{b}{c} \eta_n\right) & -J_1\left(\frac{b}{c} \eta_n\right) & -Y_1\left(\frac{b}{c} \eta_n\right) \\ 0 & 0 & J_1(\eta_n) & Y_1(\eta_n) \end{bmatrix}^{-1} \begin{bmatrix} K_1 J_1\left(\gamma_1 \frac{a}{c} \eta_n\right) \\ 0 \\ 0 \\ 0 \end{bmatrix} \tag{10}$$

Eq. (10) can be solved for each n , with the corresponding non-dimensional eigenvalue η_n substituted so that the calculation of the coefficients is purely an arithmetic exercise. The eigenfunctions are then fully determined by Eq. (6). The solution for the temperature in the homogeneous problem is then given as

$$T_i(r, t) = \frac{1}{N_0} A_0^2 \left\{ \frac{k_1}{\alpha_1} \int_0^a r' f_1(r') dr' + \frac{k_2}{\alpha_2} \int_a^b r' f_2(r') dr' + \frac{k_3}{\alpha_3} \int_b^c r' f_3(r') dr' \right\} +$$

$$N_n = \frac{k_1}{\alpha_1} \int_0^a r' [\psi_{1n}(r')]^2 dr' + \frac{k_2}{\alpha_2} \int_a^b r' [\psi_{2n}(r')]^2 dr' + \frac{k_3}{\alpha_3} \int_b^c r' [\psi_{3n}(r')]^2 dr', \tag{11b}$$

$n = 1, 2, 3, \dots$

and

$$N_0 = \frac{A_0^2}{2} \left[\frac{k_1}{\alpha_1} a^2 + \frac{k_2}{\alpha_2} (b^2 - a^2) + \frac{k_3}{\alpha_3} (c^2 - b^2) \right] = \frac{A_0^2}{2} \Delta, \tag{11c}$$

where the thermal capacitance per unit length is defined as

$$\Delta = \frac{k_1}{\alpha_1} a^2 + \frac{k_2}{\alpha_2} (b^2 - a^2) + \frac{k_3}{\alpha_3} (c^2 - b^2). \quad (11d)$$

The temperature is written in terms of the Green's function as

$$\begin{aligned} T_i(r, t) = & \int_0^a r' G_{i1}(r, t|r', \tau)|_{\tau=0} f_1(r') dr' \\ & + \int_a^b r' G_{i2}(r, t|r', \tau)|_{\tau=0} f_2(r') dr' \\ & + \int_b^c r' G_{i3}(r, t|r', \tau)|_{\tau=0} f_3(r') dr' \end{aligned} \quad (12)$$

Comparison of these two results provides the Green's function for the problem. It is given by

$$\begin{aligned} G_{ij}(r, t|r', \tau)|_{\tau=0} \\ = \frac{k_j}{\alpha_j} \left(\frac{2}{\Delta} + \sum_{n=1}^{\infty} \frac{1}{N_n} \exp(-\beta_n^2 t) \psi_{in}(r) \psi_{jn}(r') \right) \end{aligned} \quad (13)$$

where, Δ is given by Eq. (11d). The full Green's function is obtained by replacing t with $(t - \tau)$ in Eq. (13), namely,

$$\begin{aligned} G_{ij}(r, t|r', \tau) = \frac{k_j}{\alpha_j} \left(\frac{2}{\Delta} + \sum_{n=1}^{\infty} \frac{1}{N_n} \right. \\ \left. \times \exp(-\beta_n^2 (t - \tau)) \psi_{in}(r) \psi_{jn}(r') \right). \end{aligned} \quad (14)$$

For the original non-homogeneous problem, the solution may now be written down using the Greens function just calculated. It is

$$\begin{aligned} T_i(r, t) = T_0 \left\{ \int_0^a r' G_{i1}(r, t|r', \tau)|_{\tau=0} dr' \right. \\ + \int_a^b r' G_{i2}(r, t|r', \tau)|_{\tau=0} dr' \\ + \left. \int_b^c r' G_{i3}(r, t|r', \tau)|_{\tau=0} dr' \right\} \\ + \frac{\alpha_3}{k_3} \int_0^t [r' G_{i3}(r, t|r', \tau)]_{r'=c} q''(\tau) d\tau. \end{aligned} \quad (15a)$$

From the case where $q''(t) = 0$ (the homogeneous solution with uniform temperature everywhere), the temperature remains constant at T_0 . Therefore, it is deduced that the terms inside the braces $\{ \}$ in Eq. (15a) sum to unity. Then the temperature is given

simply by

$$\begin{aligned} T_i(r, t) = T_0 + \frac{\alpha_3}{k_3} \int_0^t [r' G_{i3}(r, t|r', \tau)]_{r'=c} q''(\tau) d\tau \\ = T_0 + c \int_{\tau=0}^t \left[\frac{2}{\Delta} + \sum_{n=1}^{\infty} \frac{\psi_{in}(r) \psi_{3n}(c)}{N_n} \right. \\ \left. \times \exp(-\beta_n^2 (t - \tau)) \right] q''(\tau) d\tau. \end{aligned} \quad (15b)$$

3. Results

3.1. Constant applied heat flux

For a constant applied heat flux q'' , after substituting for the Green's function and performing the integration, the solution to the problem is

$$T_i(r, t) = T_0 + cq'' \left[\frac{2}{\Delta} t + \sum_{n=1}^{\infty} \frac{\psi_{in}(r) \psi_{3n}(c)}{N_n} \frac{1}{\beta_n^2} (1 - e^{-\beta_n^2 t}) \right]. \quad (16)$$

Since $T(r, t) - T_0$ is a product of cq'' , the temperature rise in the evaporator at a given time, as well as the temperature difference between any two points, is a linear function of the applied heat flux q'' . This result is significant because it allows for the elimination of a parameter from the functional form and indicates that the temperature increase is linearly dependent on the applied heat flux.

The initial temperature T_0 and the term $cq'' \frac{2}{\Delta} t$, which corresponds to the bulk average temperature rise of the entire evaporator due to the addition of heat, can be subtracted from both sides of Eq. (16). The summation on the right-hand side is the relative transient, spatial temperature variation across the evaporator. This is then normalized by the product cq'' , which is proportional to the heat rate per unit length of the evaporator. The result is given by

$$\begin{aligned} T_i^*(r, t) \equiv \frac{T_i(r, t) - T_0}{cq''} - \frac{2}{\Delta} t \\ = \sum_{n=1}^{\infty} \frac{\psi_{in}(r) \psi_{3n}(c)}{N_n} \frac{1}{\beta_n^2} (1 - e^{-\beta_n^2 t}). \end{aligned} \quad (17)$$

A plot of the normalized temperature profile $T^*(r, t)$ is presented in Fig. 4 for a 16 mm nominal o.d. (0.633 in.) and a 30 mm nominal o.d. (1.170 in.) evaporator with ultra high molecular weight (UHMW) polyethylene wicks, and for a nickel wick evaporator with 16 mm nominal o.d. Plotting the temperature rise in its

normalized form allows a single set of curves to be used to calculate the actual temperature for any heat flux, whereas a separate plot would be necessary for each heat flux case if the actual temperature rise were plotted directly. The selected evaporator sizes represent common designs that have been tested in ground and flight experiments. For the nickel wick evaporator the thermal properties of the liquid-saturated wick and the pure liquid differ by approximately by one order of magnitude and hence the groove geometry in this case will more significantly affect the accuracy of the results. On the other hand, the properties are close to two orders of magnitude lower than those of the metal wall. In any event, it is informative to compare the results of the model using the nickel wick evaporator with those of the polyethylene wick evaporator.

The thermal property data and dimensions used in the analysis of these evaporators are given in Table 1. The effective thermal conductivity data used for the liquid-saturated wick were calculated using the following correlation [13]:

$$k_m = k_s^{1-\varphi} k_f^\varphi, \tag{18a}$$

where φ is the porosity of the wick, and k_f and k_s are the thermal conductivities of the liquid in the void space of the wick and the pure solid which forms the structure of the wick, respectively. The mixture thermal diffusivity was calculated as [13]

$$\alpha_m = \frac{k_m}{(\rho c_p)_m}, \tag{18b}$$

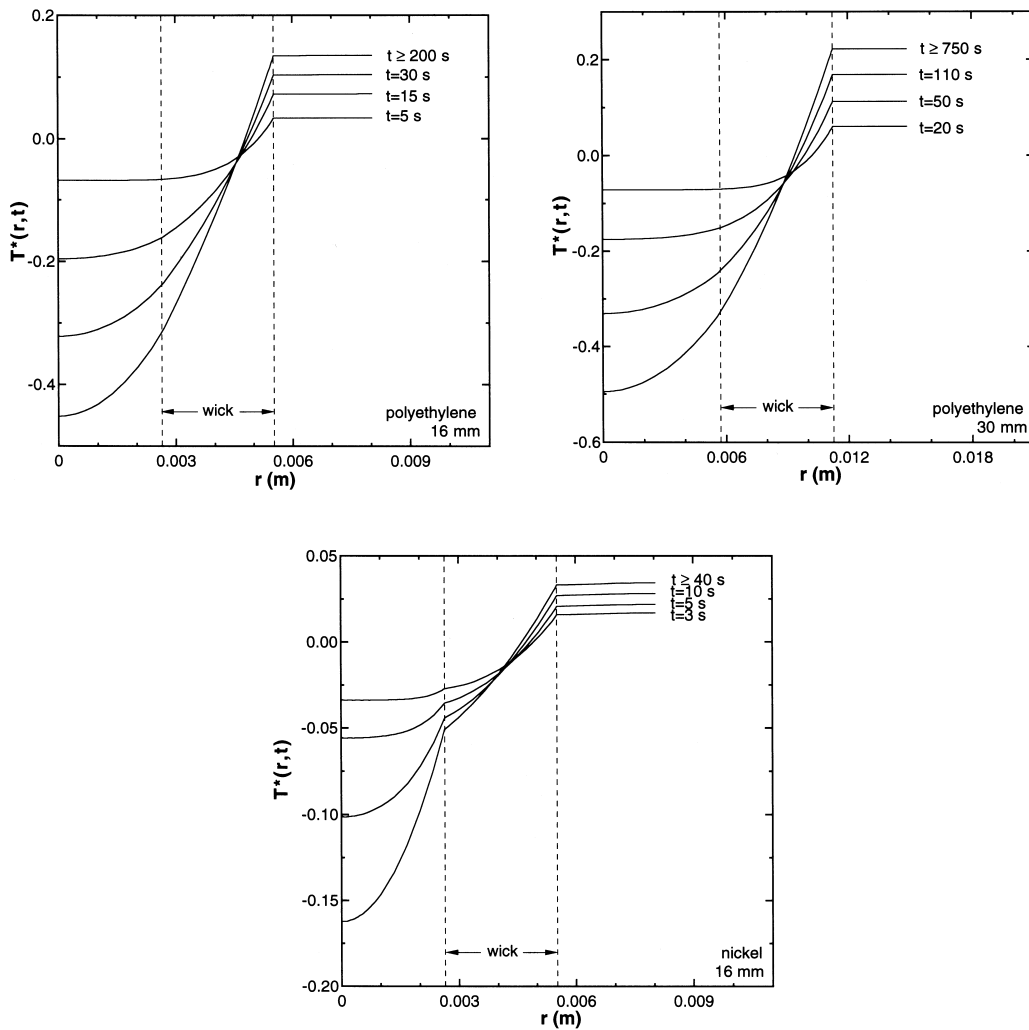


Fig. 4. Normalized temperature $T^*(r, t)$ for several times: (a) 16 mm polyethylene wick evaporator, (b) 30 mm polyethylene wick evaporator, (c) 16 mm nickel wick evaporator.

Table 1
Evaporator dimensions and thermal properties used in model

	16 mm polyethylene wick evaporator	30 mm polyethylene wick evaporator	16 mm nickel wick evaporator
Material 1	Liquid ammonia	Liquid ammonia	Liquid ammonia
a (mm)	2.64	5.72	2.64
k_2 (W/m K)	0.50	0.50	0.50
$\alpha_1 \times 10^6$ (m ² /s)	0.175	0.175	0.175
Material 2	UHMW polyethylene wick saturated with liquid ammonia	UHMW polyethylene wick saturated with liquid ammonia	Nickel alloy wick saturated with liquid ammonia
b (mm)	5.52	11.25	5.52
ϕ , wick porosity	0.50	0.50	0.70
k_s , bulk thermal conductivity of wick material, (W/m K)	0.33	0.33	90
k_2 (W/m K)	0.41	0.41	2.37
$\alpha_s \times 10^6$, bulk thermal diffusivity of wick material, (m ² /s)	0.155	0.155	22.7
$\alpha_2 \times 10^6$ (m ² /s)	0.16	0.16	0.74
Material 3	Aluminum 6063, T6	Aluminum 6063, T6	Aluminum 6063, T6
c (mm)	8.04	14.86	8.04
k_3 (W/m K)	201	201	201
$\alpha_3 \times 10^6$ (m ² /s)	83	83	83

where the mixture effective density–specific heat product is obtained as

$$(\rho c_p)_m = (1 - \phi)(\rho c_p)_s + \phi(\rho c_p)_f, \quad (18c)$$

where the subscripts f and s again refer to the fluid and pure solid, respectively.

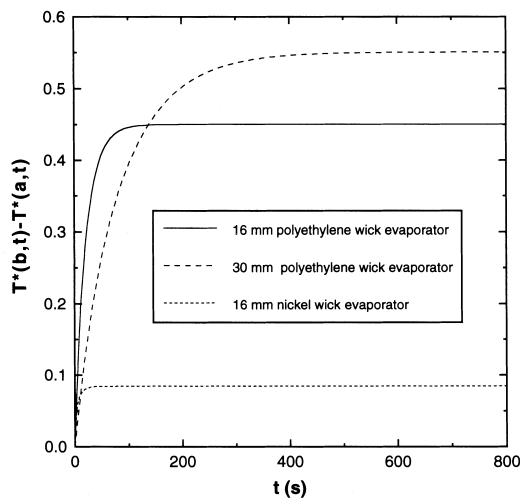


Fig. 5. Normalized temperature difference between the vapor groove location ($r = b$) and the interface between the wick and liquid core ($r = a$) for the 16 mm polyethylene wick evaporator, the 30 mm polyethylene wick evaporator, and the 16 mm nickel wick evaporator.

As can be seen from Eq. (17), a thermally fully developed condition develops as $t \rightarrow \infty$. The time at which negligible change in the thermal profile occurs depends on the magnitude of the eigenvalues β_n . For the 16 mm evaporator, for times greater than about 200 s, the temperature profile was found to become invariant, while for the 30 mm evaporator the corresponding time increased to about 750 s. As one would expect, for the larger diameter and lower thermal conductivity evaporators, the thermal diffusion time is greater. For the nickel wick evaporator, the time needed to obtain a fully developed condition decreased to only 40 s and the temperature differences are considerably smaller.

For a capillary evaporator, the temperature difference between the vapor grooves (corresponding to the interface at $r = b$) and the liquid/wick interface (corresponding to $r = a$) is of interest. If this temperature difference in an evaporator is less than the level of superheat present at the time nucleation occurs in the vapor grooves, then nucleation may also occur in the wick or liquid core. Also, if vapor is injected into the core due to a pressure spike or surge during startup, should the liquid core be near saturation when nucleation occurs, the injected vapor can remain in the core without condensing, thereby increasing the chance of an eventual evaporator deprime.

A comparison of this temperature difference for the three evaporators is presented in Fig. 5. For the 30 mm polyethylene wick evaporator, the normalized tem-

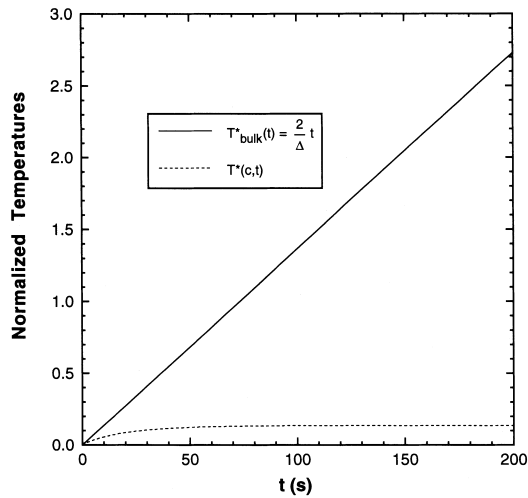


Fig. 6. Comparison of the evaporator bulk average and surface temperature rise for the 16 mm polyethylene wick evaporator for the case of a constant heat flux.

perature difference starts out smaller than that of the 16 mm polyethylene wick evaporator, but as time increases the temperature difference becomes greater for the larger evaporator. The variation of the actual temperature difference between the two evaporators is actually greater than Fig. 5 suggests, since the normalizing constant includes c , the outer radius of the evaporator. This increase in the temperature difference between the vapor grooves and liquid core, along with the increased resistance to vapor penetration through a thicker wick, may be one reason for observed improvements in startup success for large evaporators [9]. The nickel wick evaporator shows a significant reduction in the temperature difference since heat is more efficiently conducted to the liquid core. This fact, from the point of view of maintaining subcooling in the liquid core both during startup and in steady operation, makes the nickel wick evaporator an inferior design to evaporators using a traditional polyethylene wick.

3.2. The case where a thermal mass dissipates heat and is conductively coupled to the evaporator

In applications where a capillary evaporator is used, a spacecraft mission for example, there is typically a heat dissipating mass of non-negligible thermal capacitance that is conductively coupled to the evaporator. Because of the thermal capacitance of the mass and the finite conductance between the evaporator and the thermal mass, the heat flow to the evaporator is less than the heat dissipated in the mass, and a temperature difference exists between the two. The resulting non-steady heat flow to the evaporator will affect the development of the temperature profile within the evaporator.

The condition of a constant heat flux results when the thermal capacitance of the mass is negligible, as in the case of a small electric heater. This is frequently used in laboratories as a simulation of a heat dissipating payload, but it does not represent the actual service conditions of the evaporator heating, and may result in unexpected results in the startup behavior when a mass with considerable thermal capacitance replaces a simulation heater. In the following analysis, a heat flux corresponding to the heating situation of a massive thermal payload is derived, and the resulting temperature profile is calculated for a range of parameters. The results are compared with those from the case of a constant applied heat flux from the previous section.

Consider an evaporator that is conductively coupled to a thermal mass which dissipates heat at a constant rate \dot{Q} . The heat transfer in this case results in a conjugate conduction problem. The appropriate boundary condition at the evaporator surface is the following:

$$k_3 \frac{\partial T_3}{\partial r} \Big|_{r=c} = U(T_m(t) - T_3(r=c, t)) \quad (19)$$

where U is the overall heat transfer coefficient at the evaporator from the thermal mass, and $T_m(t)$ is the time-dependent temperature of the thermal mass. The thermal mass temperature, assuming it behaves as a lumped capacitance, is governed by the following differential equation

$$C_m \frac{dT_m}{dt} = \dot{Q} - UA_e(T_m(t) - T_3(c, t)) \quad (20)$$

where A_e is the evaporator area over which heat enters the evaporator, and C_m is the total thermal capacitance of the thermal mass.

The solution of a conjugate heat conduction problem, such as that given by Eqs. (1), (2a)–(2e), (19) and (20), results in an eigenvalue problem for which no orthogonality condition exists to determine the coefficients in the resulting eigenfunction expansion [14]. This causes substantial difficulty in obtaining an analytical solution. On the other hand, Eq. (15b) provides a solution to the problem if the resulting heat flux $q''(t)$ into the evaporator can be determined. This is obtained as

$$q''(t) = U(T_m(t) - T_3(r=c, t)) \quad (21)$$

by equating Eqs. (2f) and (19). Although $T_m(t)$ and $T_3(c, t)$ are obtained by solving the conjugate conduction problem and therefore are not known a priori, the following approximate analysis provides a function $q''(t)$ which yields temperature profiles that are valid for large values of time.

Consider the temperature solution for the case of a

constant applied flux, given by Eq. (16). For relatively large times, the transient temperature at the outer radius, $T_3(c, t)$, is dominated by the bulk average temperature increase $\frac{2}{\Delta}cq''t$. That is, the bulk average temperature rise of the evaporator eventually becomes much larger than the local temperature differences across the evaporator, as shown in Fig. 6 for the case of the 30 mm polyethylene wick evaporator. In the case of the second heating condition, the heat flux will be reduced and the evaporator surface temperature will therefore not rise as quickly as in the case of a constant heat flux. The temperature variation across the evaporator therefore, may be neglected and the bulk average temperature is used as a reasonable approximation for the evaporator surface temperature $T_3(c, t)$. This is equivalent to assuming a lumped capacitance for the evaporator, which is used only in determining the approximate heat flux into the evaporator when it is conductively coupled to an external heat dissipating thermal mass.

With the above discussion as motivation, the conduction problem of two lumped capacitances, the evaporator and a thermally dissipating mass, which are thermally coupled through a constant heat transfer coefficient U , is solved. Specifically, the differential equations obtained from an energy balance on the lumped masses are solved. For the thermal mass,

$$\dot{Q} - A_e U(T_m(t) - T_e(t)) = C_m \frac{dT_m}{dt}, \quad (22a)$$

while for the evaporator

$$A_e U(T_m(t) - T_e(t)) = C_e \frac{dT_e}{dt}. \quad (22b)$$

As initial condition, it is assumed that both masses are at the same temperature,

$$T_m(t=0) = T_e(t=0) = T_0. \quad (22c)$$

The heat flux to the evaporator, in the lumped mass approximation, is given by

$$q''(t) = U(T_m(t) - T_e(t)). \quad (23)$$

Solving the two differential equations, Eqs. 22(a) and 22(b), in terms of the heat flux results in the following:

$$\begin{aligned} q''(t) &= \frac{\dot{Q}C_e}{A_e(C_m + C_e)} \left[1 - \exp\left(-\frac{C_m + C_e}{C_m} \frac{A_e U}{C_e} t\right) \right] \\ &= \frac{\dot{Q}}{A_e(1 + R_c)} [1 - \exp(-\xi t)], \end{aligned} \quad (24a)$$

where

$$R_c = \frac{C_m}{C_e} \quad (24b)$$

is the ratio of thermal capacitances and

$$\xi = \frac{1 + R_c}{R_c} \frac{UA_e}{C_e}. \quad (24c)$$

The function given by Eq. (24a) is the approximate transient heat flux into the evaporator resulting from a conductive coupling to a heat dissipating, lumped capacitance thermal mass. Substituting this approximate heat flux into Eq. (15b) and performing the integration yields the temperature of the evaporator due to this heating condition,

$$\begin{aligned} T_i(r, t) &= T_0 + \frac{\dot{Q}}{A_e} \frac{c}{1 + R_c} \left\{ \frac{2}{\Delta} \left[t - \frac{1}{\xi} (1 - e^{-\xi t}) \right] \right. \\ &\quad + \sum_{n=1}^{\infty} \frac{\psi_{in}(r)\psi_{3n}(c)}{N_n} \frac{1}{\beta_n^2 - \xi} \left[(1 - e^{-\xi t}) \right. \\ &\quad \left. \left. - \frac{\xi}{\beta_n^2} (1 - e^{-\beta_n^2 t}) \right] \right\}. \end{aligned} \quad (25)$$

Normalizing the result in a similar manner as in the case of a constant heat flux, it is found that

$$\begin{aligned} T_i^*(r, t, \xi) &= \frac{T_i(r, t) - T_0}{c \left(\frac{\dot{Q}}{A_e} \right) \left(\frac{1}{1 + R_c} \right)} - \frac{2}{\Delta} \left[t - \frac{1}{\xi} (1 - e^{-\xi t}) \right] \\ &= \sum_{n=1}^{\infty} \frac{\psi_{in}(r)\psi_{3n}(c)}{N_n} \frac{1}{\beta_n^2 - \xi} \\ &\quad \left[(1 - \exp(-\xi t)) - \frac{\xi}{\beta_n^2} (1 - \exp(-\beta_n^2 t)) \right]. \end{aligned} \quad (26)$$

Eq. (26) reduces to the case of constant heat flux when $\xi \rightarrow \infty$. In practice, for values of ξ that are quite small it is found that the normalized temperature profiles obtained from Eq. (26) still do not vary substantially from those obtained in the case of a constant heat flux (Eq. (17)). For example, only when $\xi < 0.1$ does the difference in the normalized temperature become noticeable in the case of the 16 mm polyethylene wick evaporator. This result becomes obvious upon examining the factor multiplying the term

$$\frac{\psi_{in}(r)\psi_{3n}(c)}{N_n}$$

for the $T^*(r, t)$ and $T_i^*(r, t, \xi)$ profiles of Eqs. (17) and (26), respectively. A plot of the time dependent factor

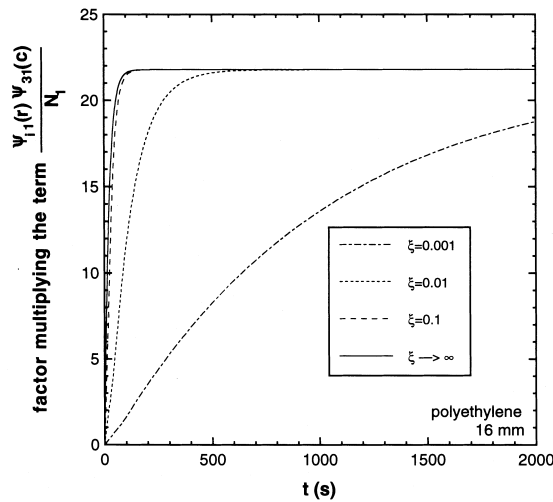


Fig. 7. Factor multiplying the term $\psi_{11}(r)\psi_{31}(c)/N_1$ in Eq. (26) for the 16 mm polyethylene wick evaporator.

$$\frac{1}{\beta_1^2 - \xi} \left[(1 - \exp(-\xi t)) - \frac{\xi}{\beta_1^2} (1 - \exp(-\beta_1^2 t)) \right],$$

corresponding to $n = 1$, for the case of the 16 mm evaporator appears in Fig. 7 for various values of ξ , where $\xi \rightarrow \infty$ represents the coefficient appearing in Eq. (17). A plot of the resulting temperature profiles for $\xi = 0.01$, shown in Fig. 8, may be compared with Fig. 4(a). Clearly, a shift in the time at which a fully developed profile occurs results for the smaller ξ value but the shape of the normalized temperature profiles does not vary significantly. As $t \rightarrow \infty$, the two profiles are identical, as may be derived from the equations.

In practice, the parameter ξ will be small enough to effect a change in the temperature profile only when the thermal conductance from the source is quite small. The area of the evaporator in contact with a cold plate may be approximated as the product of the diameter and active length of the evaporator. As an example, consider a typical, if conservative, heat transfer coefficient U of $4000 \text{ W/m}^2 \text{ K}$, corresponding to an aluminum-to-aluminum thermal contact under a contact pressure of 1000 kN/m^2 in vacuum [15]. For a 16 mm evaporator with a length of 30 cm, it is calculated from Eq. (24c) that $\xi \geq 0.4$ for any value of R_c . Since both the evaporator area A_e and the capacitance C_e are proportional to the length, the value of ξ can decrease below 0.1 only if there is a significant decrease in the total heat transfer coefficient U . The normalized bulk temperature rise of the evaporator also does not change significantly from the constant heat flux case for $\xi \geq 0.1$ except at very early times. Therefore, in most cases, the T^* profiles can be determined using the limiting value $\xi \rightarrow \infty$, which corresponds to the functional form of Eq. (17).

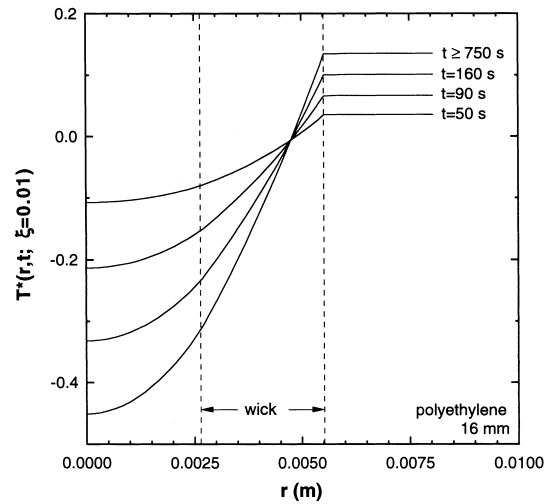


Fig. 8. Normalized temperature $T^*(r, t; \xi = 0.01)$ for the case of the 16 mm polyethylene wick evaporator for several times.

As an example of the degree of attenuation of the temperature profile due to the presence of the thermal mass, consider an evaporator with the properties of the 16 mm polyethylene wick evaporator from Table 1. Assuming a length of 38.1 cm (15 in.), with a 38.1 cm \times 10.2 cm \times 0.6 cm aluminum cold plate attached, the capacitance ratio is slightly above ten. From Fig. 5 one observes a maximum normalized temperature difference between the vapor grooves and the liquid core of 0.45. For a heat dissipation rate of 100 W, the rate per area of the evaporator is approximately 5.2 kW/m^2 . When this flux is applied directly to the evaporator without a cold plate, the maximum actual temperature difference between the grooves and the liquid core is calculated from Eq. (16) to be 37.5°C . For the same evaporator with the cold plate attached and the same heating rate, assuming negligible additional thermal capacitance, the maximum temperature difference is found to be only $37.5^\circ\text{C}/(1+10) = 3.4^\circ\text{C}$. This provides motivation for avoiding the use of a cold plate in a dedicated starter pump and minimizing its thermal mass when a fully flooded startup will be used with any evaporator design.

3.3. Temperature difference between vapor grooves and liquid core at boiling incipience as a function of heat flux

In the previous calculation for a constant flux applied to an evaporator without a cold plate, the maximum temperature difference was calculated as 37.5°C . However, if the initial temperature T_0 is only a few degrees below the saturation temperature (reservoir setpoint), nucleation will occur before the calcu-

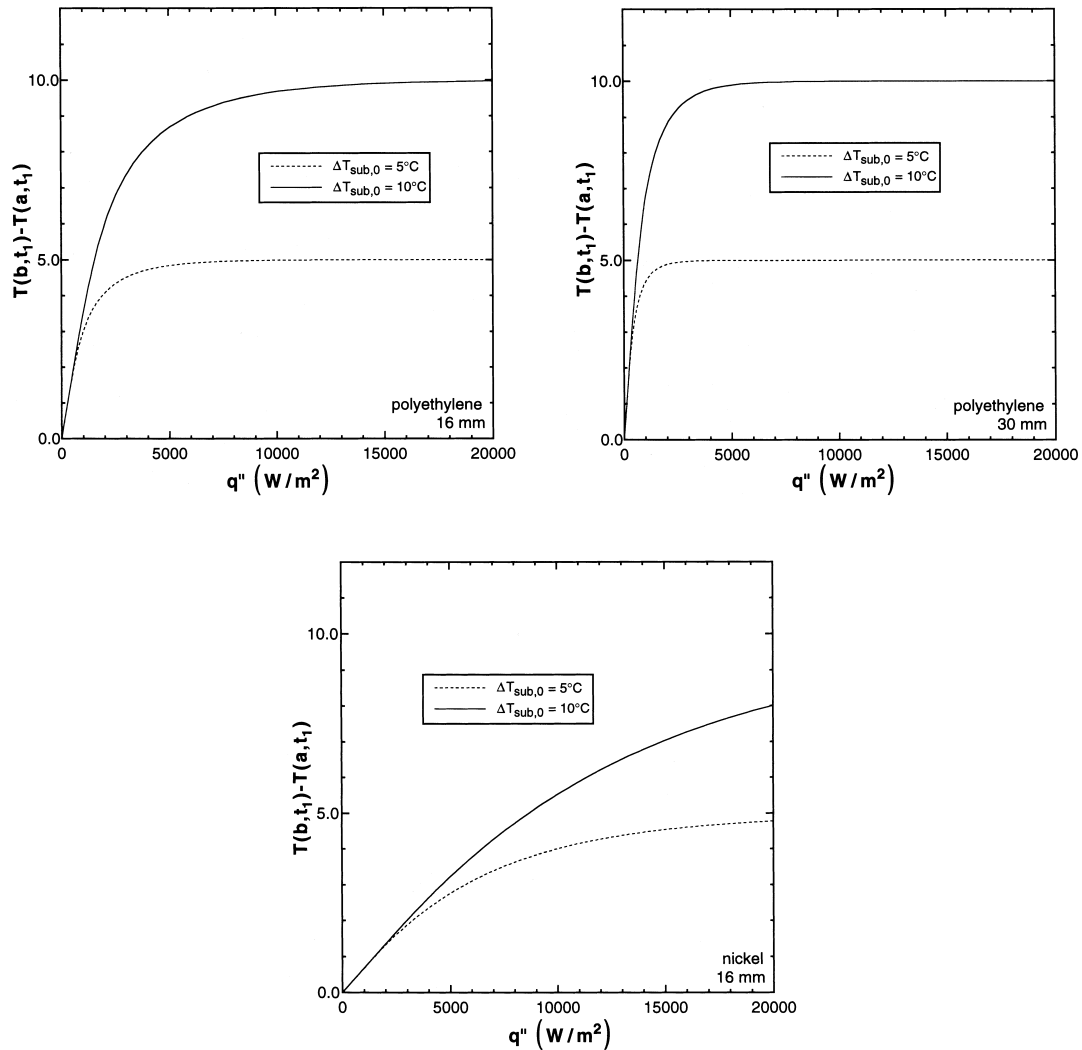


Fig. 9. Difference in temperature between the vapor grooves and the wick–liquid interface at the time $t = t_1$ when nucleation is expected, plotted as a function of the applied heat flux q'' for (a) the 16 mm polyethylene wick evaporator, (b) the 30 mm polyethylene wick evaporator, and (c) the 16 mm nickel wick evaporator.

lated maximum temperature difference can be reached. Therefore, the maximum temperature difference is limited by the initial subcooling $\Delta T_{sub,0} = T_{sat} - T_0$, neglecting incipient superheat. Superheating could easily be included in the following analysis by using the expected nucleation temperature instead of the saturation temperature specified here.

In order to start an evaporator it is desirable to simply apply power to the device from which the evaporator is intended to reject heat. However, this procedure may not result in a successful startup. To maximize the probability of a successful startup, it is necessary to maintain a comfortable temperature difference between the vapor grooves and the liquid core, and as seen in the previous analysis, this may

be achieved by applying a sufficiently large heat flux to the evaporator. The addition of dedicated starter heaters may be justified in some circumstances. On the other hand, if too large of a heat flux is applied to the evaporator in an effort to maximize the vapor groove–wick temperature difference, other complications may result in the startup being unsuccessful. A larger heat flux than necessary will cause the boiling/evaporation immediately following nucleation to be more vigorous and a larger pressure surge can be expected as a result. If the pressure surge is too large, vapor may be injected through the wick into the liquid core, which may result in startup failure. Therefore, the applied heat flux should be selected so that sufficient subcooling

remains in the core at nucleation, but vapor generation rates corresponding to that flux should not exceed the wick's capability to accelerate fluid through the rest of the loop.

It is desirable to know the temperature difference at the moment nucleation occurs in the vapor grooves, expressed as a function of the applied heat flux. The first nucleation event occurs at the time t_1 when

$$T(b, t_1) = T_{\text{sat}}, \quad (27)$$

where the function $T(b, t)$ is obtained from Eq. (16). In terms of the function

$$\tilde{T}_b(t) = \frac{2}{\Delta}t + T^*(b, t), \quad (28)$$

t_1 is the time at which

$$\tilde{T}_b(t_1) = \frac{\Delta T_{\text{sub}, 0}}{cq''}. \quad (29)$$

One can show that the function \tilde{T}_b has an inverse, so t_1 is obtained as

$$t_1 = \tilde{T}_b^{-1}\left(\frac{\Delta T_{\text{sub}, 0}}{cq''}\right). \quad (30)$$

Of primary interest is the value of

$$T(b, t_1) - T(a, t_1) = cq''\Delta T_{\text{gc}}^*(t_1), \quad (31)$$

where

$$\Delta T_{\text{gc}}^*(t) = T^*(b, t) - T^*(a, t) \quad (32)$$

is the normalized temperature difference between the vapor grooves and the liquid core. From Eq. (30), t_1 may be written as a function of the heat flux, $t_1 = t_1(q'')$. Therefore, the actual vapor groove to liquid core temperature difference at boiling incipience is obtained as a function of q'' as

$$\begin{aligned} \Delta T_{\text{gc, incip}}(q'') &= T(b, t_1) - T(a, t_1) \\ &= cq''\Delta T_{\text{gc}}^*(t_1(q'')). \end{aligned} \quad (33)$$

The temperature difference of interest is plotted as a function of q'' for initial subcoolings of 5 and 10°C in Fig. 9 for the three evaporators discussed previously. For the 30 mm polyethylene wick evaporator a lower flux is required to maintain the same level of subcooling in the liquid core at boiling incipience as compared to the smaller diameter polyethylene wick evaporator, a fact which has been observed experimentally at NASA, Goddard [9]. The nickel wick evaporator requires a considerably higher heat flux to maintain the same level of liquid core subcooling. These figures show an important trend which is particularly relevant

to the discussion at the beginning of this section concerning high power startups. This is that there exists a flux limit beyond which there is no substantial increase in the temperature difference between the vapor grooves and the liquid core. Any further increase in applied power for a given initial subcooling only results in an increased pressure surge during vapor channel clearing, with no thermal differences that will improve the likelihood of a successful startup.

4. Conclusions

A thermal model was developed to determine the temperature profile during the heating stage before nucleation occurs in the vapor grooves of a flooded capillary evaporator. The boundary conditions of an applied constant heat flux and conduction to a thermally dissipating lumped mass with non-negligible thermal capacitance were considered. The temperature difference between the vapor grooves and liquid core was examined with a focus on practical methods to maintain a suitable level of subcooling in the liquid core. Key conclusions of this investigation are as follows:

1. The transient relative thermal profile in an evaporator during the preheating stage is linearly dependent upon the applied heat flux.
2. The presence of a large thermal mass seriously reduces the temperature differences present in an evaporator during the preheat stage of a startup because the heat dissipated in the thermal mass is transferred to the evaporator in proportion to the relative thermal capacitances of the evaporator and thermal mass. Dedicated starter heaters attached directly to the evaporator or starter pumps become a practical necessity if the liquid core subcooling is to be maintained when a large thermal mass is present.
3. Thermal differences between small and large diameter evaporators during the preheat stage were examined and the likelihood of startup success was considered. Results of this analysis were in agreement with experimental observations and trends. Large evaporators can start more easily since the added thermal resistance to the liquid core results in an increase in the level of subcooling present there in the fully developed temperature profile.
4. Wicks with a higher thermal conductivity significantly reduce the level of subcooling in the liquid core. Heat fluxes several times greater than those needed for polyethylene wicks are required to maintain the same subcooling when a metal wick evaporator is used.
5. The temperature difference between the vapor

grooves and the liquid/wick interface can be predicted with this model. A minimum heat flux needed to produce a comfortable level of subcooling in the liquid core at boiling incipience can be calculated so that nucleation cannot occur in the liquid core and any bubbles that may be injected into the core can be condensed.

Acknowledgements

The authors are grateful for the support of the Office of Basic Energy Sciences of the U.S. Department of Energy (Grant No. DE-FG02-93ER14394.A003). Financial support for the first author was provided through the Air Force Palace Knight Program. The authors also would like to express their appreciation to Dr. Donald Gluck of Texas A and M University, Center for Space Power, for his comments and suggestions.

References

- [1] B.A. Cullimore, Capillary pumped loop application guide, SAE Paper 932156, 1993.
- [2] J. Ku, Overview of capillary pumped loop technology. HTD-Vol. 236, in: Proceedings of the 29th National Heat Transfer Conference, Atlanta, GA, 1993, pp. 1–17.
- [3] J. Ku, Recent advances in capillary pumped loop technology, AIAA Paper 97-3870, 1997.
- [4] T.T. Hoang, J. Ku, Theory of hydrodynamic stability for capillary pumped loops. HTD-Vol. 307, in: Proceedings of the 1995 National Heat Transfer Conference, Vol. 5, Portland, OR, 1995, pp. 33–40.
- [5] T. Hoang, J. Ku, Hydrodynamic aspects of capillary pumped loops, SAE Paper 961435, 1996.
- [6] T. Hoang, Development of an advanced capillary pumped loop, SAE Paper 972325, 1997.
- [7] J.H. Kim, K. Cheung, D. Butler, J. Ku, E. Haught, E.J. Krolczek, B. Cullimore, J. Baumann, The capillary pumped loop III (CAPL III) flight demonstration description and status, in: Proceedings of the Space Technology and Applications International Forum, Albuquerque, NM, 1997, pp. 623–628.
- [8] B.A. Cullimore, Start-up transients in capillary pumped loops, AIAA Paper 91-1374, 1991.
- [9] J. Ku, Start-up issues of capillary pumped loops. Advances in Heat Pipe Science and Technology, in: Proceedings of the 9th International Heat Pipe Conference, Albuquerque, NM, 1995, pp. 994–1001.
- [10] J. Ku, T. Hoang, T. Nguyen, S. Yun, Performance tests of CAPL 2 starter pump cold plates, AIAA Paper 96-1837, 1996.
- [11] T. Li, J.M. Ochterbeck, Effect of wick thermal conductivity on startup of a capillary pumped loop evaporator, AIAA paper 99-3446, Proceedings of the 33rd Thermophysics Conference, Norfolk, VA, 1999.
- [12] M.N. Özisik, Heat Conduction, Wiley, New York, 1980.
- [13] D.A. Nield, A. Bejan, Convection in Porous Media, Springer-Verlag, New York, 1992.
- [14] R.E. Langer, A problem in diffusion or in the flow of heat for a solid in contact with a fluid, *Tôhoku Mathematical Journal* 35 (1932) 260–275.
- [15] E. Fried, Thermal conduction contribution to heat transfer at contacts, in: R.P. Tye (Ed.), Thermal Conductivity, vol. 2, 1969, pp. 253–274.